Radiatively coupled waveguide polarization splitter simulated by wave-matching based coupled mode theory

M. Lohmeyer, N. Bahlmann, O. Zhuromskyy, P. Hertel*
Department of Physics, University of Osnabrück,
Barbarastraße 7, D-49069 Osnabrück, Germany

Abstract: Coupled mode theory is applied to an arrangement of three raised strip waveguides with a multimode central strip. We use semivectorial numerically computed modes of the three single isolated waveguides as a basis for a propagating supermode analysis of the entire structure. The pronounced polarization dependence of the raised strip guides allows for the design of a conveniently short polarization splitter. We discuss design guidelines and estimate the fabrication tolerances. The accuracy of the coupled mode approach is assessed by comparison with rigorously computed supermodes for comparable two waveguide couplers. Both types of structures indicate the limits in the applicability of the coupled mode model.

Keywords: integrated optics, dielectric waveguides, numerical modeling, coupled mode theory, polarization splitter
PACS codes: 42.82.–m 42.82.Et

1 Introduction

Radiative coupling [1] has been shown a mean to achieve power transfer between remote parallel waveguides in an integrated optics chip. A three waveguide arrangement as sketched in Fig. 1 with two identical outer guides and a broad strip in between may be viewed as two leaky waveguides, where the power radiated by one waveguide is caught by the opposite one. This motivates the term radiative coupling and perturbational simulations based on leaky modes [1, 2].

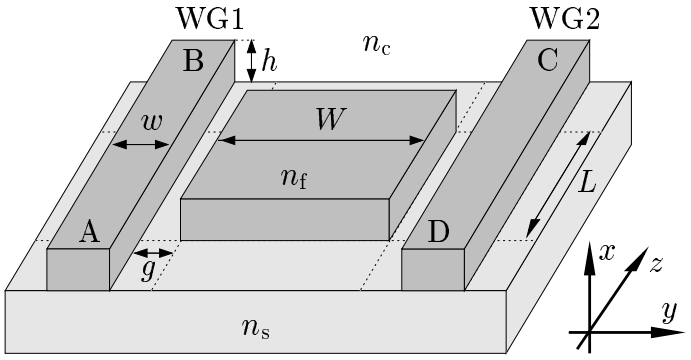

Figure 1: Three waveguide coupler geometry. The central strip couples the two identical outer waveguides WG1 and WG2 along a distance L. The structures are to be considered four port devices with input and output channels A to D.

Planar three waveguide coupling characteristics (cf. [3, 4, 5] and references cited therein) were studied e.g. for the purpose of wavelength filtering [6]. As well as for polarization splitting [2], planar radiatively coupled waveguides have been simulated for use as optical isolators [7] or for nonlinear switching [8]. The particular advantage of these structures is the lack of waveguide bends. Only longitudinally homogeneous waveguide sections are involved, and this is convenient both for design and manufacturing.

To date, however, there seems to be no investigation of etched rib- or strip waveguide based devices, as presented in this paper. We do not stress the viewpoint of radiative coupling, but consider the entire coupler structure as one single lossless waveguide. Interference of its supermodes determines the coupling behaviour. In simulations of analogous planar devices [2, 7] one can observe an almost periodical dependence of the supermode propagation constants on the spacing between the outer waveguides. Along with the mode wavenumbers, the characteristic

*Fachbereich Physik, Universität Osnabrück Barbarastraße 7, D 49069 Osnabrück
Tel.: +541/969-2641 Fax: +541/969-2670 e-mail: manfred.lohmeyer@physik.uni-osnabrueck.de

length for the power transfer varies periodically with the waveguide distance. One obtains a polarization splitter if the device length can be adjusted to be an even (odd) multiple of the coupling length for TE polarization and to be an odd (even) multiple of the length for TM polarized light. The shortest device results if the coupling length for TE polarized light is at its maximum while at the same time the TM length is minimal, or vice versa.

The structures are to be modeled by means of coupled mode theory [9, 10, 11]. For one of the standard formulations, Secs. 2 and 3 recall the basic equations and their solution in terms of supermodes. To assess the accuracy level that can be expected in the following calculations, the first part of Sec. 4 compares the coupled mode theory results with rigorous data, for a series of conventional two-waveguide couplers. Finally Sec. 4.2 reports on the results regarding the polarization splitter design.

As we have demonstrated in [12], an analysis based on directly computed supermodes is feasible as well which avoids the approximations introduced by the coupled mode theory. However, for a complete design usually a large number of simulations are required. Besides a prohibitive demand of computing power, the direct procedure becomes unreliable due to the need to calculate higher order modes with closely spaced propagation constants. At least this difficulty can be overcome with the considerably faster coupled mode theory approach.

2 Coupled mode theory

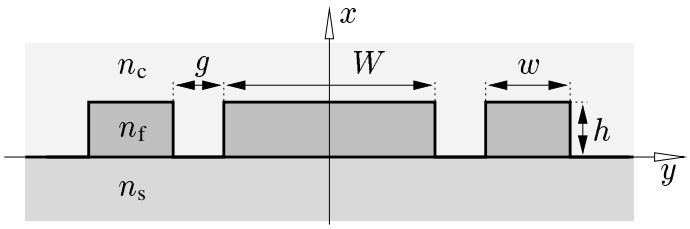

Figure 2: Cross section of the three waveguide coupler. Parameters are the strip height h, the widths of the central strip W and of the outer guides w, and the permittivities $\epsilon_s = n_s^2$, $\epsilon_f = n_f^2$, $\epsilon_c = n_c^2$, of the substrate, the guiding film, and the cover material, respectively. x and y denote the cross section coordinate axes, with the y-direction parallel to the substrate surface. Light propagates along the z-axis.

Fig. 2 sketches the basic geometry under investigation. For a simulation in the framework of coupled mode theory, we suppose the guided modes of the three single waveguides to be known. For fixed polarization, these are the two single modes of the outer waveguides, and the set of modes of the central guide. They are represented by their electric and magnetic field profiles $\boldsymbol{E}_m = (E_{m,x}, E_{m,y}, \mathrm{i}E_{m,z})$, $\boldsymbol{H}_m = (H_{m,x}, H_{m,y}, \mathrm{i}H_{m,z})$, with real components $E_{m,x}$, ..., $H_{m,z}$ depending on the transverse coordinates only. The total guided electromagnetic field $\boldsymbol{\mathcal{E}}$, $\boldsymbol{\mathcal{H}}$ is assumed to be a superposition

$$\boldsymbol{\mathcal{E}}(x,y,z,t) = \sum_m C_m(z) \frac{1}{\sqrt{P_m}} \boldsymbol{E}_m(x,y)\, \mathrm{e}^{\mathrm{i}\omega t}, \quad \boldsymbol{\mathcal{H}}(x,y,z,t) = \sum_m C_m(z) \frac{1}{\sqrt{P_m}} \boldsymbol{H}_m(x,y)\, \mathrm{e}^{\mathrm{i}\omega t} \tag{1}$$

of the single modes, normalized by $P_m = \iint (E_{m,x} H_{m,y} - E_{m,y} H_{m,x})\, \mathrm{d}x\, \mathrm{d}y/2$, with coefficients C_m which include the harmonic dependence on the propagation distance. β_m denotes the propagation constant at a frequency ω corresponding to the vacuum wavelength λ and wavenumber $k = 2\pi/\lambda = \omega\sqrt{\epsilon_0 \mu_0}$ for vacuum permittivity ϵ_0 and permeability μ_0.

Each mode is assigned the difference $\Delta\epsilon_m = \epsilon - \epsilon_m$ between the permittivity profile ϵ (in general a tensor) describing the entire three-guide structure and the permittivity ϵ_m, with which mode number m was calculated. From Maxwell's equations the following reciprocity identity can be derived straightforwardly [13]:

$$\mathrm{div}(\boldsymbol{\mathcal{H}} \times \boldsymbol{\mathcal{E}}_m^* - \boldsymbol{\mathcal{E}} \times \boldsymbol{\mathcal{H}}_m^*) = \mathrm{i}\omega\epsilon_0 \boldsymbol{\mathcal{E}}_m^* \, \Delta\epsilon_m \boldsymbol{\mathcal{E}} \,. \tag{2}$$

$\boldsymbol{\mathcal{E}}_m$ and $\boldsymbol{\mathcal{H}}_m$ are the mode profiles $\boldsymbol{E}_m$, $\boldsymbol{H}_m$ multiplied by the appropriate time and space dependence $\exp(\mathrm{i}\omega t - \mathrm{i}\beta_m z)$. Integration over the x-y-plane and insertion of (1) yields

$$\sum_l \sigma_{ml} (\partial_z C_l + \mathrm{i}\beta_m C_l) = -\mathrm{i} \sum_l \alpha^{\mathrm{I}}_{ml} C_l \tag{3}$$

with the power coupling coefficients σ_{lm} defined as

$$\sigma_{lm} = \frac{1}{4\sqrt{P_l P_m}} \iint (E_{l,x} H_{m,y} - E_{l,y} H_{m,x} + E_{m,x} H_{l,y} - E_{m,y} H_{l,x}) \,\mathrm{d}x \,\mathrm{d}y \tag{4}$$

and for

$$\alpha^{\mathrm{I}}_{lm} = \frac{\omega\epsilon_0}{4\sqrt{P_l P_m}} \iint \boldsymbol{E}_l^* \,\Delta\epsilon_l \boldsymbol{E}_m \,\mathrm{d}x \,\mathrm{d}y \,. \tag{5}$$

Obviously $\sigma_{lm} = \sigma_{ml}$ holds, but in general the coupling coefficients α^{I}_{lm} are not symmetric. One can invoke the reciprocity theorem a second time [13], now in the form

$$\mathrm{div}(\boldsymbol{\mathcal{H}}_l \times \boldsymbol{\mathcal{E}}_m^* - \boldsymbol{\mathcal{E}}_l \times \boldsymbol{\mathcal{H}}_m^*) = \mathrm{i}\omega\epsilon_0 \boldsymbol{\mathcal{E}}_m^* \,(\epsilon_l - \epsilon_m) \boldsymbol{\mathcal{E}}_l \,, \tag{6}$$

to show the identity

$$(\beta_l - \beta_m)\sigma_{lm} = \alpha^{\mathrm{II}}_{lm} - \alpha^{\mathrm{I}}_{lm} \quad \text{with} \quad \alpha^{\mathrm{II}}_{lm} = \frac{\omega\epsilon_0}{4\sqrt{P_l P_m}} \iint \boldsymbol{E}_l^* \,\Delta\epsilon_m \boldsymbol{E}_m \,\mathrm{d}x \,\mathrm{d}y \,. \tag{7}$$

If inserted into Eq. (3), this leads to

$$\sum_l \sigma_{ml}(\partial_z C_l + \mathrm{i}\beta_l C_l) = -\mathrm{i} \sum_l \alpha^{\mathrm{II}}_{ml} C_l \tag{8}$$

Combination of Eqs. (3) and (8) yields coupled mode equations with symmetrical coupling matrices

$$\sum_l \sigma_{ml} \partial_z C_l = -\mathrm{i}\frac{1}{2} \sum_l \sigma_{ml}(\beta_m + \beta_l) C_l - \mathrm{i} \sum_l \kappa_{ml} C_l \,, \tag{9}$$

where the coupling coefficients κ_{lm} are defined as

$$\kappa_{lm} = \frac{\omega\epsilon_0}{8\sqrt{P_l P_m}} \iint \boldsymbol{E}_l^* \,(\Delta\epsilon_l + \Delta\epsilon_m) \boldsymbol{E}_m \,\mathrm{d}x \,\mathrm{d}y \,. \tag{10}$$

For lossless materials ϵ, ϵ_m are Hermitian, thus $\kappa^*_{ml} = \kappa_{lm}$. In matrix form the coupled mode equations read

$$\mathsf{S}\partial_z \boldsymbol{C} = -\mathrm{i}(\mathsf{B} + \mathsf{K})\boldsymbol{C} \tag{11}$$

with real symmetric matrices $\mathsf{S} = (\sigma_{lm})$, $\mathsf{B} = (\sigma_{lm}(\beta_l + \beta_m)/2)$, and Hermitian $\mathsf{K} = (\kappa_{lm})$, acting on the vector $\boldsymbol{C} = (C_l)$ of mode amplitudes.

The total guided power $P = \mathrm{Re} \iint (\boldsymbol{\mathcal{E}} \times \boldsymbol{\mathcal{H}}^*)_z \,\mathrm{d}x \,\mathrm{d}y/2$ evaluates to $P = \boldsymbol{C}^\dagger \mathsf{S} \boldsymbol{C}$, where † denotes the adjoint. Its vanishing derivative $\partial_z P = \mathrm{i}\boldsymbol{C}^\dagger \left\{ (\mathsf{B} + \mathsf{K})^\dagger - (\mathsf{B} + \mathsf{K}) \right\} \boldsymbol{C}$ indicates that Eqs. (9) conserve power.

3 Supermode propagation

Eq. (11) is readily solved by an ansatz of harmonic dependence on the propagation distance, $\boldsymbol{C}(z) = \boldsymbol{a}\,\mathrm{e}^{-\mathrm{i}\beta z}$, where $\boldsymbol{a}$ is a constant weighting vector and β is the supermode propagation constant. For purely real permittivities this ansatz leads to the real generalized eigenvalue problem

$$(\mathsf{B} + \mathsf{K})\boldsymbol{a} = \beta \mathsf{S} \boldsymbol{a} \,. \tag{12}$$

If only forward propagating modes are included in (1), positive S permits convenient numerical solution of (12) via Cholesky-decomposition of S [14]. The solution consists of a number of supermode propagation constants β^s and corresponding real vectors $\boldsymbol{a}^s$ which constitute the supermode field profiles

$$\boldsymbol{E}^s = \sum_m a^s_m \frac{1}{\sqrt{P_m}} \boldsymbol{E}_m \,, \quad \boldsymbol{H}^s = \sum_m a^s_m \frac{1}{\sqrt{P_m}} \boldsymbol{H}_m \,. \tag{13}$$

For nondegenerate propagation constants, the orthogonality property $(\boldsymbol{a}^r)^\top \mathsf{S} \boldsymbol{a}^s = \delta_{rs} P^s$ holds, where P^s is the power assigned to supermode number s, and $\delta_{rs} = 1$ for $r = s$, otherwise $\delta_{rs} = 0$. This can be written $(\boldsymbol{E}^r, \boldsymbol{H}^r; \boldsymbol{E}^s, \boldsymbol{H}^s) = \delta_{rs} P^s$, with the symmetrical product of two sets of mode profiles defined as

$$(\boldsymbol{E}^r, \boldsymbol{H}^r; \boldsymbol{E}^s, \boldsymbol{H}^s) = \frac{1}{4} \iint (E_x^r H_y^s - E_y^r H_x^s + E_x^s H_y^r - E_y^s H_x^r) \, \mathrm{d}x \, \mathrm{d}y \,. \tag{14}$$

The field in the homogeneous coupling section has the form (1) with coefficients

$$C_m(z) = \sum_s A^s \frac{1}{\sqrt{P^s}} a_m^s \, \mathrm{e}^{-\mathrm{i}\beta^s z}, \tag{15}$$

i.e. a supermode superposition with constant amplitudes A^s:

$$\boldsymbol{\mathcal{E}}(x,y,z,t) = \sum_s A^s \frac{1}{\sqrt{P^s}} \boldsymbol{E}^s(x,y) \, \mathrm{e}^{\mathrm{i}\omega t - \mathrm{i}\beta^s z}, \quad \boldsymbol{\mathcal{H}}(x,y,z,t) = \sum_s A^s \frac{1}{\sqrt{P^s}} \boldsymbol{H}^s(x,y) \, \mathrm{e}^{\mathrm{i}\omega t - \mathrm{i}\beta^s z}. \tag{16}$$

Supermode orthogonality allows to express the total guided power in the coupling region as $P = \sum_s |A^s|^2$.

Now we come back to the three waveguide coupler structure. At $z = 0$, the simulation shall start with the single mode field $\sqrt{P_\mathrm{in}/P_i}\,(\boldsymbol{E}_i, \boldsymbol{H}_i)$ of one outer waveguide (index i), scaled to an input power P_in. This input field is assumed to be well represented by the supermodes. Neglecting radiation and reflection, projection on the supermode fields (13) with respect to (14) yields the amplitudes

$$A^s = \sqrt{\frac{P_\mathrm{in}}{P^s}} \sum_m \sigma_{im} a_m^s \,. \tag{17}$$

For $z > L$, coupling vanishes. Only the modes of the single outer waveguides remain, and for these we can assume $(\boldsymbol{E}_j, \boldsymbol{H}_j; \boldsymbol{E}_k, \boldsymbol{H}_k) = \delta_{jk} P_k$ due to the waveguide separation. Neglecting radiation and reflection again, the power output P_out^l is given by projection on the output mode number l. The result is

$$P_\mathrm{out}^l = P_\mathrm{in} \left| \sum_s \frac{1}{P^s} \left(\sum_m \sigma_{lm} a_m^s \right) \left(\sum_m \sigma_{im} a_m^s \right) \mathrm{e}^{-\mathrm{i}\beta^s L} \right|^2 , \tag{18}$$

completely analogous to the expression for planar couplers [7], if the sums over m are viewed as products (14) between supermode s and the input respectively output field.

4 Numerical results

We employed the semivectorial version of a recently proposed mode solver [15] to compute mode fields and propagation constants for the single, unperturbed waveguides and to generate the reference data for the two-waveguide couplers. The method is based on local plane wave expansions for regions with constant permittivity. The semianalytical mode fields are not limited to a computational window. They take the continuity requirements at dielectric interfaces explicitely into account and allow for a convenient analytical evaluation of the various integrals that arise from the coupled mode theoretical treatment.

For our simulations we chose parameters typical for magnetic garnets [16]: YIG-films, $n_\mathrm{f} = 2.2$, epitaxially grown on GGG substrates, $n_\mathrm{s} = 1.95$. The wavelength is set to a value of $\lambda = 1.3\,\mu$m.

4.1 Two waveguide couplers

Omitting the center strip in Fig. 2 establishes a conventional directional coupler. If viewed as one longitudinal homogeneous waveguide, the structure supports two guided modes of opposite symmetry, with slightly different propagation constants β_s, β_a. Power is transfered between the two cores on a distance of one half beat length $L_\mathrm{c} = \pi/(\beta_\mathrm{s} - \beta_\mathrm{a})$. Fig. 3 compares results for L_c and β_s, β_a from direct mode calculations and values obtained by supermode composition via coupled mode theory.

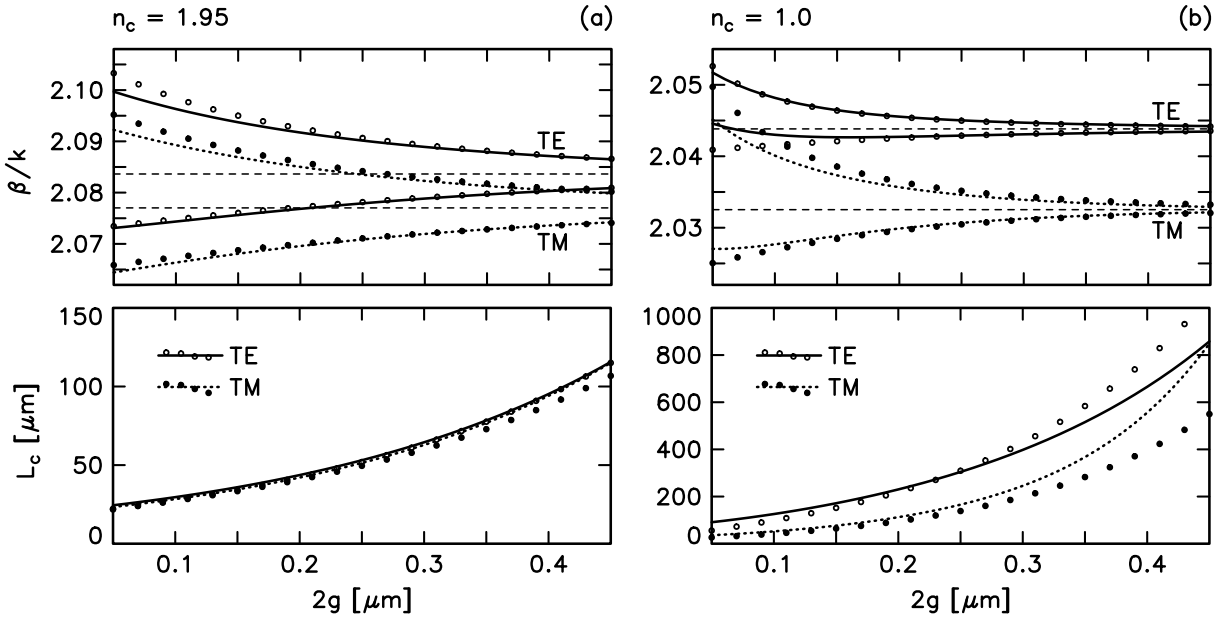

Figure 3: Effective mode indices (top) and coupling length L_c (bottom) versus strip spacing $2g$ for two waveguide couplers as in Fig. 2 with $W = 0$, and $n_c = n_s$ (a) or $n_c = 1.0$ (b). Lines mark coupled mode theory results, while marker symbols show values from direct supermode calculations. The horizontal lines in the top charts indicate the levels of the single waveguides propagation constants. Parameters are $h = 0.7\ \mu$m and $w = 1.2\ \mu$m; remaining values are given in the text.

Charts (a) correspond to embedded waveguides covered by the substrate material, charts (b) to uncovered waveguides. There is good agreement in the propagation constants, with larger deviations occurring only for increased coupling at smaller gap width. Although coupling is stronger for the embedded waveguides, as indicated by the shorter coupling length, deviations in the propagation constants are less pronounced due to the lower permittivity contrast between the core and the gap regions. We conclude, that we have implemented the perturbational theory adequately.

However, while simulating the less strongly guiding structures should be somewhat more reliable, they are less sensitive to the polarization. The difference between the levels of TE and TM propagation constants increases with growing contrast between the core and cover permittivities. According to the bottom charts of Fig. 3, the difference between the TE and TM coupling lengths is also significantly larger for gap refractive index $n_c = 1.0$ than for $n_c = n_s$. Aiming at a short total length, the polarization splitter design should be based on structures with high permittivity contrast. Therefore the following section deals with raised strips rather than embedded or rib waveguides.

With regard to the coupling length, the bottom part of Fig. 3 (b) shows the measure of agreement between coupled mode theory and the rigorous calculations. The results agree best for gap spacings between $0.1\ \mu$m and $0.25\ \mu$m. Deviations for small gaps should be due to the larger field strength, and thus larger errors, of the coupled mode fields in the gap region. As illustrated by Fig. 4, the deviations for L_c at large gap width are accompanied by an excellent agreement of the coupled mode theory mode profiles with rigorously computed fields.

However, for large core separation with large coupling length, the propagation constants of the symmetric and antisymmetric supermodes converge, while we must assume a certain fixed numerical error for both the directly computed values β_s, β_a and the basic profiles for the isolated waveguides. The former affect the accuracy of our reference results, the latter influence the coupled mode theory. Obviously one cannot expect an agreement in the limit of large waveguide separation, as it is the case for planar step index waveguides, where analytical solutions are available.

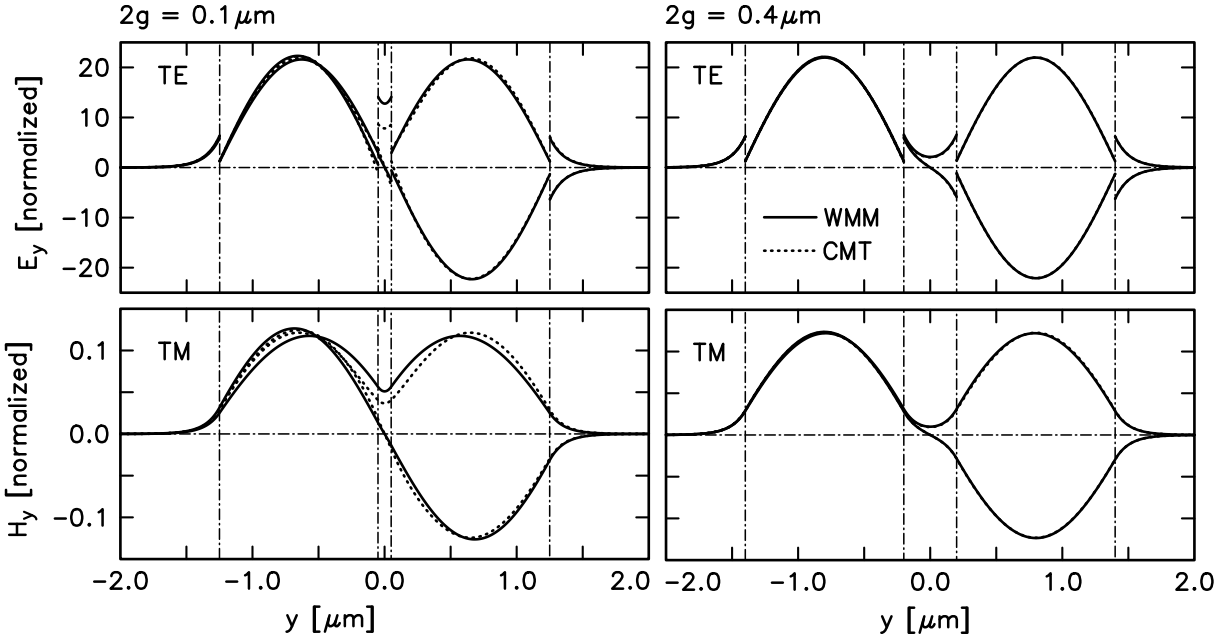

Figure 4: Mode profiles for two waveguide couplers evaluated along the horizontal line $x = 0.35\,\mu$m at half the strip height. Parameters are as given for Fig. 3(b), with the gap size $2g$ set to $0.1\,\mu$m (left) and $0.4\,\mu$m (right). Top charts are for TE, bottom charts for TM polarization. The continuous lines show the directly calculated supermodes, dotted lines correspond to supermode profiles composed by coupled mode theory.

4.2 Three waveguide polarization splitter

Our simulations start with the computation of the guided modes sets for a series of isolated central waveguides, for varying width W. With the two additional modes of the outer waveguides with fixed geometries and gap width, the coupled mode analysis for the three waveguide coupler yields supermode dispersion curves as shown in Fig. 5.

The supermode propagation constants exhibit the expected asymptotic behaviour. For proper polarization and height, the wavenumbers of the corresponding planar, three layered waveguides constitute upper limits. The propagation constant β_* of the isolated outer waveguides is indicated by the central thin horizontal line. Outside the region around this level, the supermode dispersion curves resemble the lines for the isolated central waveguide of the same width.

The corresponding mode profiles exist on the central core only, with small amplitudes on the outer core regions, as illustrated by the mode profiles in Fig. 6. In contrast, the supermodes with propagation constants close to β_* have only small amplitudes on the core region of the central waveguide, but larger field strength on the outer cores. In the example of Fig. 6, these are the three supermodes of order 4, 5, and 6 for TE polarization and those of 4th and 5th order for TM polarization.

All these findings agree with the expectations from our investigations on planar structures [2, 7], and with the results of rigorous supermode calculations [12]. At the same time, from planar simulations one would expect β_* to match the region of almost horizontal tangents in the supermode dispersion curves. As shown by the magnifications in the right part of Fig. 5, this regions turn out to be shifted upwards from the levels β_*. This observation is confirmed by the rigorous treatment.

If the structure is excited by the single waveguides modes, the supermodes with large amplitudes on the outer cores, i.e. those with propagation constants close to β_*, will carry the main part of the inserted power. This allows to define a characteristic coupling length as $L_\mathrm{c} = |\beta^\mathrm{s} - \beta^\mathrm{a}|$, where β^s, β^a are the wavenumbers of the symmetric (s) and antisymmetric (a) supermodes with largest initial weights Eq. (17). Constructive interference of these two modes is at least a necessary condition for the power transfer between the outer waveguides. This condition covers the distribution of the largest part of the guided power. Note that for complete power transfer the remaining modes must add properly to the two most dominant, and this additional constraint is not included in the definition of L_c.

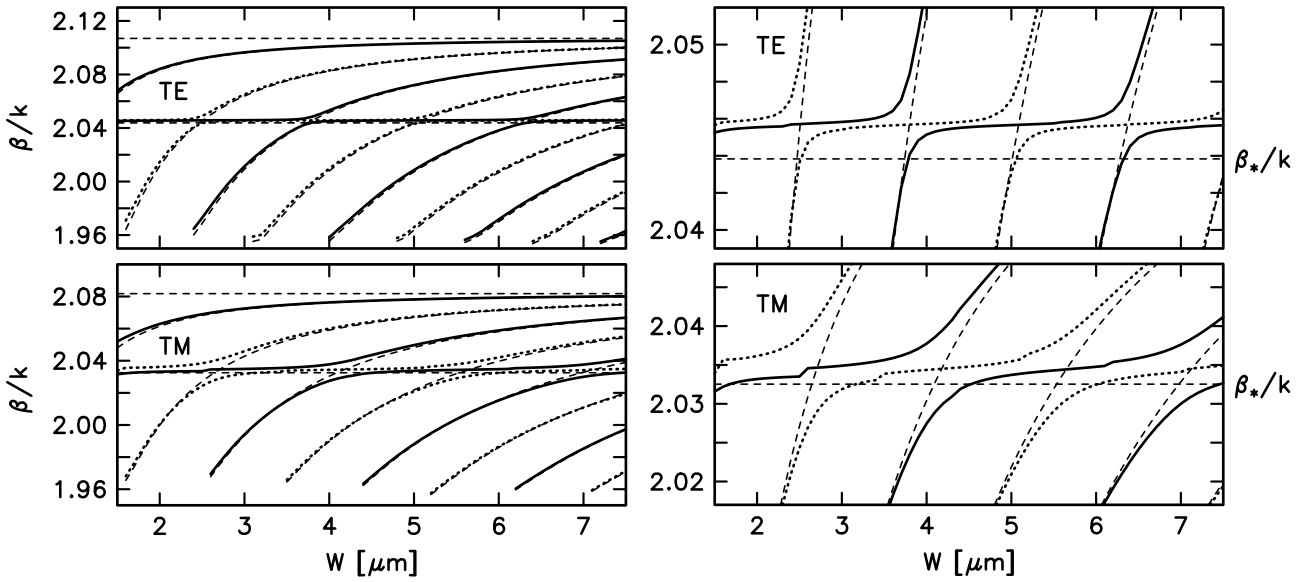

Figure 5: Effective mode indices β/k for the supermodes of the three waveguide coupler, for TE (top) and TM polarization (bottom), and for supermodes of even (continuous lines) and odd symmetry (dotted lines), versus the width W of the central waveguide. The thin dashed lines indicate the effective mode indices of the corresponding planar waveguide (top line), the levels β_*/k of the modes of the isolated outer waveguides (center line) and the mode indices of the isolated center guide of proper width. Paramters are $h = 0.7\,\mu$m, $w = 1.2\,\mu$m, $g = 0.1\,\mu$m, other values as given in the text.

For our series of couplers L_c evaluates to the curves of Fig. 7. The figure confirms the pronounced difference between the TE and TM coupling behaviours as predicted in Sec. 4.1. The curves are not smooth due to two reasons. First, in the locations of the minima, the supermodes change, which enter the expression for L_c.

The second reason for the discontinuity becomes apparent, if Figs. 7 and 5 are compared. With increasing width W, the basic set of coupled modes is enlarged by newly appearing modes of the central rib. These are identified by the mode solver only if there is a certain distance between the trial propagation constant and the background value, given by the substrate refractive index. If a guided mode is identified, its field distribution (which enters the coupled mode theory integrals) becomes more and more unreliable for a mode approaching cutoff. Even if the accuracy can be increased, with numerically calculated basic modes there will never be a smooth transition to enlarged mode sets. We regard this as a fundamental problem for the application of coupled mode theory to such multimode structures. However, while a quantitative accuracy better than the discontinuities in $L_\mathrm{c}(W)$ cannot be guaranteed, the qualitative behaviour of these curves is correct. We can expect reliable results at least for the orders of magnitudes in the total length and fabrication tolerances for devices investigated by the coupled mode theory model.

For the following design we stick to a region away from the discontinuities for both TE and TM. We have assumed the waveguide height, wavelength and refractive indices to be fixed, and calculated a series of central waveguide mode sets with $4.5\,\mu\mathrm{m} < W < 5.1\,\mu\mathrm{m}$. Then coupled mode theory simulations with parameters varying around $w = 1.2\,\mu$m, $g = 0.1\,\mu$m lead to a parameter set for a well performing polarization splitter as summarized in Table 1.

	W	w	g	h	λ	L
q	$4.96\,\mu$m	$1.21\,\mu$m	$0.11\,\mu$m	$0.70\,\mu$m	$1.30\,\mu$m	$850\,\mu$m
Δq	± 10 nm	± 1 nm	± 2 nm	± 20 nm	± 1 nm	$\pm 25\,\mu$m

Table 1: Parameters and tolerances for a three waveguide polarization splitter according to Figs. 1 and 2. See the text for the interpretation of the tolerances and for refractive index values.

The device achieves polarization splitting ratios of $\mathrm{ER}_1 = 10\log_{10}(P_\mathrm{out}^{1,\mathrm{TM}}/P_\mathrm{out}^{1,\mathrm{TE}}) = 27\,\mathrm{dB}$ and $\mathrm{ER}_2 = 10\log_{10}(P_\mathrm{out}^{2,\mathrm{TE}}/P_\mathrm{out}^{2,\mathrm{TM}}) = 26\,\mathrm{dB}$. For otherwise tuned parameters, the geometry tolerances are determined such that both ER_1 and ER_2 exceed the level 20 dB, if a parameter deviates from its optimum q by no more than

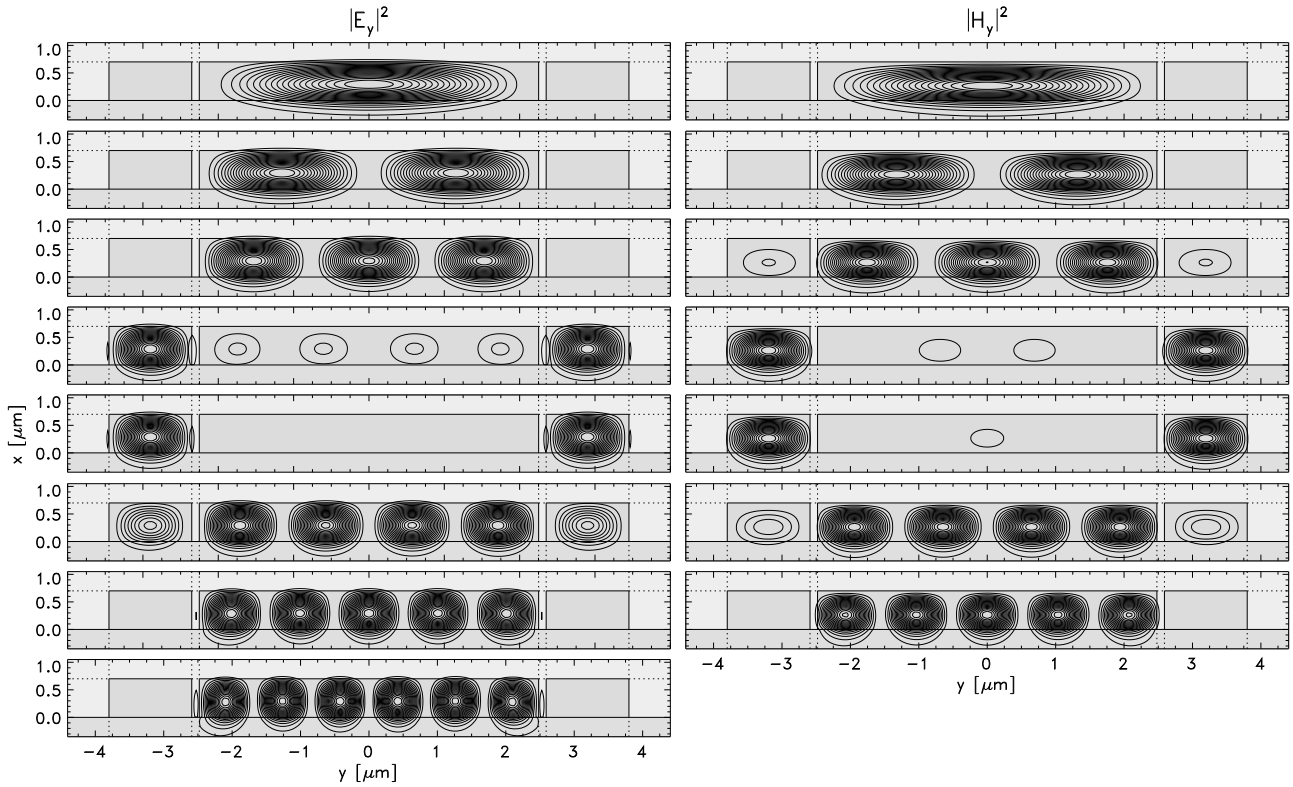

Figure 6: Mode intensity profiles for a three waveguide coupler, for TE (left) and TM polarization (right). Parameters are $h = 0.7\,\mu$m, $w = 1.21\,\mu$m, $g = 0.11\,\mu$m, $W = 4.96\,\mu$m, remaining values as given in the text.

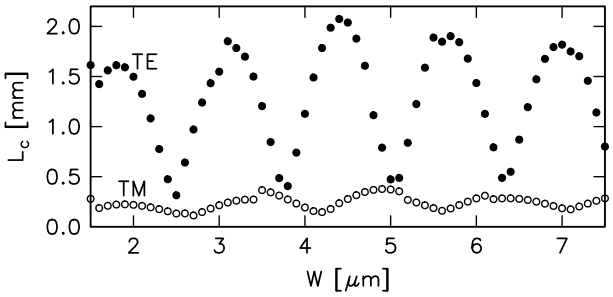

Figure 7: Coupling length for the couplers of Fig. 5, for TE (filled circles) and TM polarized light (open markers) versus the width W of the central waveguide.

the value Δq given in the table. The tolerances are roughly estimated with the help of perturbational expressions for the derivative $\partial_q \beta^s$ of propagation constants due to geometry variations [17], based on the supermode profiles of Fig. 6. For each parameter $q \in \{W, h, w, g, \lambda\}$, we have calculated curves $P_{\rm out}^{1,2;\rm TE,TM}(\delta q)$ and the extinction ratios by Eq. (18), with original mode profiles, but with the propagation constants changed by $\partial_q \beta^s \delta q$, and read off the tolerance values. Note that $\partial_\lambda \beta^s$ is connected to the derivatives with respect to the remaining length parameters by $\partial_\lambda \beta^s = -(\beta^s + w\partial_w \beta^s + W\partial_W \beta^s + g\partial_g \beta^s + h\partial_h \beta^s)$. Unfortunately the short device length has its price: the tolerances for the widths of the gaps and of the outer waveguides are very strict. At the same time, due to similar supermode profiles along the vertical direction, the waveguide height turns out to be an uncritical parameter.

The optimum device length, its tolerance and the peak performance are indicated by the curves of Fig. 8. From Fig. 7, at $W = 4.96\,\mu$m one expects a coupling length for TE beeing about twice as long as that for TM, corresponding to the superposition of the dominant modes. Despite the interference of 8 TE and 7 TM modes, this sinusoidal trend is clearly visible in the power versus propagation distance curves of Fig. 8.

Finally, Fig. 9 illustrates the light propagation in the polarization splitter. Note that for most positions $0 < z < L$ part of the power is carried in the center core region, therefore $P_{\rm out}^{1,\rm TE/TM}$ and $P_{\rm out}^{2,\rm TE/TM}$ usually do not add to one.

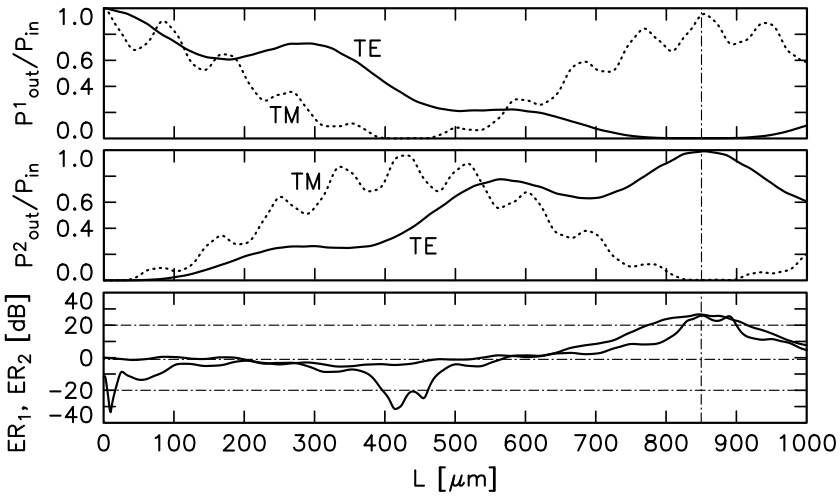

Figure 8: Relative output power for TE (continuous lines) and TM polarization (dotted lines) for waveguide WG1 (top) and waveguide WG2 (center) and extinction ratios ER_1, ER_2 (bottom) versus the length of the coupling section L. Paramters are as given for Fig. 6. The vertical line indicates the proper length for a polarization splitter.

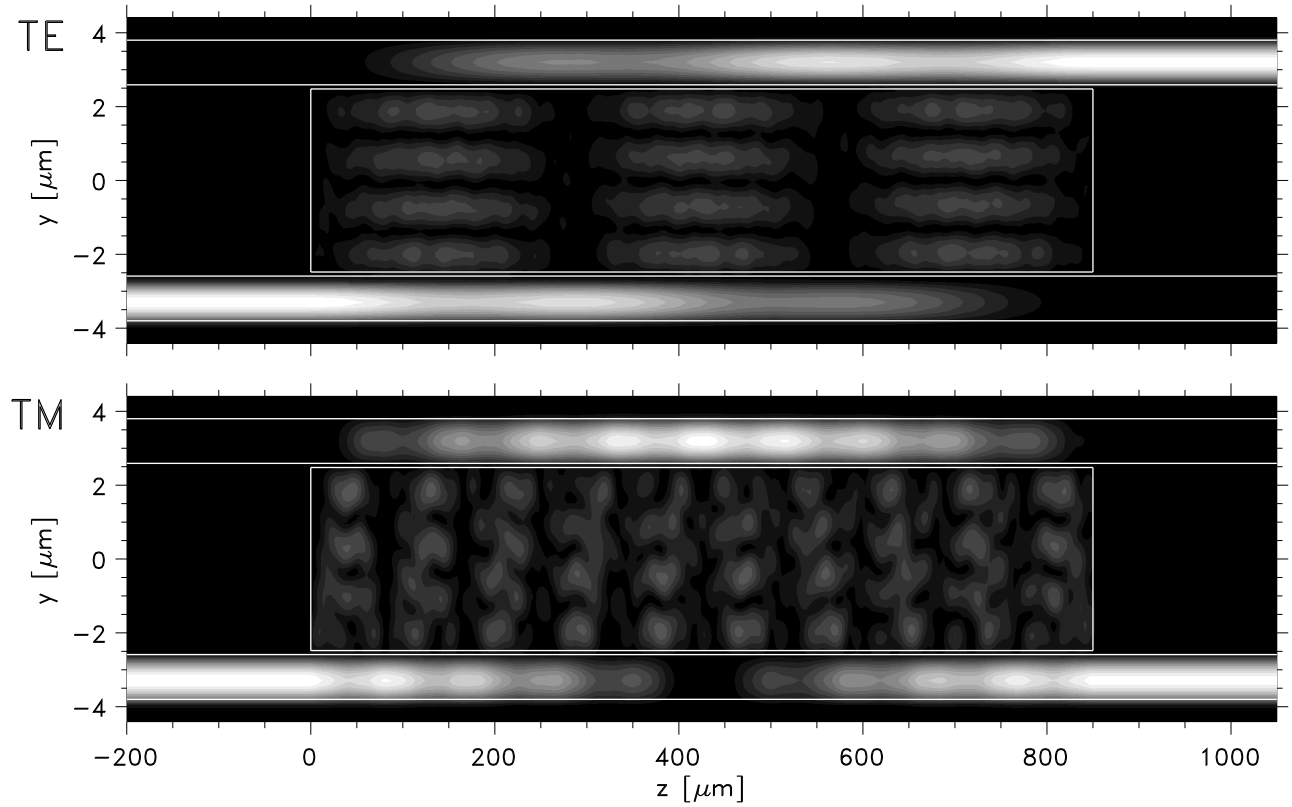

Figure 9: TE (top) and TM light propagation (bottom) for the three waveguide coupler as prescribed by the parameters of Fig. 6. The length of the coupling section is $L = 850\,\mu$m. The greyscale levels correspond to the squareroot of the z-component of the Poynting vector, evaluated in the y-z-plane at half the waveguide height $x = h/2$.

5 Conclusions

Coupled mode theory can be successfully applied to the supermode analysis of multimode and multiwaveguide raised strip structures. We have employed the wave matching method to generate quasianalytical semivectorial approximations for the basic mode sets, which allow for a convenient and direct implementation of the coupled mode formalism. Comparison with rigorously computed results for two waveguide couplers prove that the coupled mode model is adequate even for the high refractive index contrasts occurring with the raised strip geometry. This is an advantage for high polarization sensitivity.

We have found good agreement between the main features of light propagation in planar radiatively coupled waveguides and the more realistic three dimensional structures investigated in this paper. The accuracy actually achieved is sufficient to reveal the qualitative properties of the light propagation and to estimate device length

and fabrication tolerances. At the same time, high refractive index contrasts and unavoidable shortcomings of the numerically computed basic mode sets limit the applicability of the coupled mode approach.

The analysis shows that three waveguide couplers based on raised strip waveguides qualify well for the design of polarization splitters. The design yields proper splitting ratios at a total length of about 850 μm, avoiding the need for waveguide bends. Like many interference based devices, it suffers from strict fabrication tolerances.

Acknowledgment

Financial support by Deutsche Forschungsgemeinschaft (Sonderforschungsbereich 225) is gratefully acknowledged.

References

[1] S. M. Loktev, V. A. Sychugov, and B. A. Usievich. Propagation of light in a system of two radiatively coupled waveguides. *Sov. Journal of Quantum Electronics*, 24(5):435–438, 1994.

[2] M. Shamonin, M. Lohmeyer, and P. Hertel. Directional coupler based on radiatively coupled waveguides. *Applied Optics*, 36(3):635–641, 1997.

[3] J. P. Donelly. Limitations on Power Transfer Efficiency in Three-Guide Optical Couplers. *IEEE Journal of Quantum Electronics*, 22(5):610–616, 1986.

[4] K. L. Chen and S. Wang. The Crosstalk in Three-Waveguide Optical Directional Couplers. *IEEE Journal of Quantum Electronics*, 22(7):1039–1041, 1986.

[5] J. P. Donelly and H. A. Haus. Symmetric Three-Guide Optical Coupler with Nonidentical Center and Outside Guides. *IEEE Journal of Quantum Electronics*, 23(4):401–406, 1987.

[6] A. Haus and C. G. Fonstad. Three-Waveguide Couplers for Improved Sampling and Filtering. *IEEE Journal of Quantum Electronics*, 17(12):2321–2325, 1981.

[7] M. Lohmeyer, M. Shamonin, and P. Hertel. Integrated Optical Circulator based on Radiatively Coupled Waveguides. *Optical Engineering*, 36(3):889–895, 1997.

[8] M. Shamonin, M. Lohmeyer, and P. Hertel. Analysis of Power-Dependent Switching Between Radiatively Coupled Planar Waveguides. *Journal of Lightwave Technology*, 15(6):983–989, 1997.

[9] S. L. Chuang. A Coupled Mode Formulation by Reciprocity and a Variational Principle. *Journal of Lightwave Technology*, 5(1):5–15, 1987.

[10] W. P. Huang. Coupled mode theory for optical waveguides: an overview. *Journal of the Optical Society of America A*, 11(3):963–983, 1994.

[11] D. G. Hall and B. J. Thompson, editors. *Selected Papers on Coupled-Mode Theory in Guided-Wave Optics*, volume MS 84 of *SPIE Milestone Series*. SPIE Optical Engineering Press, Bellingham, Washington USA, 1993.

[12] M. Lohmeyer, M. Shamonin, N. Bahlmann, P. Hertel, and H. Dötsch. Radiatively coupled waveguide concept for an integrated magneto-optic circulator. In K. Rubin, J. A. Bain, T. Nolan, D. Bogy, B. J. H. Stadler, M. Levy, J. P. Lorenzo, M. Mansuripur, Y. Okamura, and R. Wolfe, editors, *High-Density Magnetic Recording and Integrated Magneto-Optics: Materials and Devices*, pages 519–524, 1998. MRS Symposium Proceedings Series, volume 517.

[13] C. Vassallo. *Optical Waveguide Concepts*. Elsevier, Amsterdam, 1991.

[14] W. H. Press, B. P. Flannery, S. A. Teukolsky, and W. T. Vetterling. *Numerical Recipes in C, 2nd ed.* Cambridge University Press, 1992.

[15] M. Lohmeyer. Wave-matching method for mode analysis of dielectric waveguides. *Optical and Quantum Electronics*, 29:907–922, 1997.

[16] M. Wallenhorst, M. Niemöller, H. Dötsch, P. Hertel, R. Gerhardt, and B. Gather. Enhancement of the nonreciprocal magneto-optic effect of TM modes using iron garnet double layers with opposite Faraday rotation. *Journal of Applied Physics*, 77(7):2902–2905, 1995.

[17] M. Lohmeyer, N. Bahlmann, and P. Hertel. Geometry tolerance estimation for rectangular dielectric waveguide devices by means of perturbation theory. *Optics Communications*, 1998. Submitted.